

# Rock Modeling and Matching for Autonomous Mars Rover Localization

Ron Li, Kaichang Di, Jue Wang, Shaojun He

Mapping and GIS Laboratory, CEEGS, The Ohio State University  
470 Hitchcock Hall, 2070 Neil Avenue, Columbus, OH 43210-1275  
Tel: 614-292-4303; E-mail: {li.282, di.2, wang.813, he.119}@osu.edu

Andrew Howard, Larry Matthies

Jet Propulsion Laboratory, California Institute of Technology  
Mail Stop 125-209, Pasadena, CA 91109  
E-mail: abhoward@robotics.jpl.nasa.gov, larry.matthies@jpl.nasa.gov

**Abstract** - In Mars rover missions, a high degree of accuracy in localization of the rover and mapping of the surrounding terrain is of fundamental importance for safe rover navigation and for achievement of scientific and engineering goals. In the Mars Exploration Rover (MER) 2003 mission, ground image-based incremental bundle adjustment (BA) technology has been performed on Earth to correct rover position errors caused by wheel slippage, azimuthal angle drift and other navigation errors. Key to the success of the BA is selection of a sufficient number of well-distributed tie points to link the ground images into an image network. Although tie-point selection at one rover site can be automated, much of the cross-site tie-point selection is performed manually during MER mission operations.

We are developing an innovative method to automate cross-site tie-point selection so that rover localization can be autonomously performed onboard the rover. This new method consists of algorithms for rock extraction, rock modeling, and rock matching from multiple rover sites. Rocks are extracted from 3D ground points generated by stereo image matching, and then modeled using analytical surface models including the hemispheroid, semi-ellipsoid, cone and tetrahedron. Rocks extracted and modeled from two adjacent rover sites are matched by a combination of rock-model matching and rock-distribution-pattern matching. Initial test results using MER data show that the proposed method is effective for medium-range (up to 26m) traverse segments. We are currently testing our software using data acquired in January, 2007 during a field test at Silver Lake, CA. The onboard incremental BA technology we are developing will be integrated with JPL's visual odometry technology to achieve long-range autonomous rover localization.

## I. INTRODUCTION

In the current Mars Exploration Rover (MER) 2003 mission and the future Mars Science Laboratory (MSL) 2009 mission, highly accurate determination of rover position and attitude information is very important both for safe rover navigation and for achievement of mission science and engineering goals [1][2][3]. Different positioning methodologies have been researched for mobile robot localization and navigation. These include dead-reckoning (odometry and inertial navigation) and

reference-based technologies such as the Global Positioning System (GPS), landmark navigation and model (map) matching [4]. However, some technologies cannot be applied directly to the Martian environment because of the unavailability of, e.g., GPS on Mars and limitations in payload and power.

Planetary rover localization research has been carried out at the Jet Propulsion Laboratory (JPL) using several advanced methods including position and heading estimation by remote viewing of a colored cylindrical target [5], maximum-likelihood matching of range maps [6], and visual odometry (VO) algorithms [7]. The Robotics Institute at Carnegie Mellon University (CMU) has designed and developed various robotic systems and vehicles for industry and military applications. Field experiments performed in recent years achieved a localization accuracy of 3-to-5 percent of distance traveled based on a dead-reckoning technology that integrated wheel encoders and roll and pitch inclinometers with a yaw gyro [8]. The Centre National d'Etudes Spatiales is also developing Mars rover autonomous navigation technology based on IMU (Inertial Measurement Unit), odometry and stereo vision [9]. The Mapping and GIS Laboratory at The Ohio State University (OSU), in collaboration with the JPL's Computer Vision Group, has developed a bundle adjustment (BA) method for long-range Mars rover localization using descent and rover images [2] [10].

In the Mars Pathfinder (MPF) 1997 mission, the rover Sojourner achieved an overall localization error of about 10% of the distance from the lander within an area of about 10x10 meters using dead-reckoning technology [11]. In the MER mission, the designed accuracy of 10% has been achieved by combining wheel odometry, a sun finding technique using rover images, and IMU to estimate rover positions and attitudes. The combined onboard VO and Earth-based BA method is capable of correcting position errors caused by wheel slippage, azimuthal angle drift and other navigation errors as large as the 21% error experienced within Eagle Crater (Meridiani Planum

landing site) and the 10.5% error found in the Husband Hill area (Gusev Crater landing site) [3] [12] [13] [14]. The Spirit rover has achieved an accuracy of 0.5% over a 6km traverse using this integrated VO and BA method. Key to the success of this method is selection of a sufficient number of well-distributed tie points to link the ground images into an image network. Although tie-point selection at one rover site has been automated, much of the cross-site tie-point selection is performed manually during MER mission operations.

This paper introduces the key component of autonomous BA operations, a new approach to cross-site tie-point selection based on rock extraction, rock modeling, and rock matching. Recent results of cross-site tie-point selection using MER and field test data are included.

## II. AUTOMATIC CROSS-SITE TIE-POINT SELECTION FOR AUTONOMOUS MARS ROVER LOCALIZATION

The concept and design of the new approach to autonomous long-range Mars rover localization based on integrated BA and VO methods are discussed in [15][16][17] in detail. The success of automatic long-range rover localization depends on the automation of VO and BA performed onboard the rover. In the MER mission, the onboard VO has worked successfully. Although automatic selection of the tie points at one site has been effectively performed on a routine basis [14] [18], the automatic, Earth-based BA has been limited by the challenge of automatic selection of cross-site tie points where objects (e.g., rocks) used as tie points look significantly different when viewed from different angles, especially in forward-versus backward-looking views. Therefore, it is crucial to develop cross-site tie-point selection algorithms for automatic selection of a sufficient number of high quality tie points to link all the images and to form an image network.

Across the Martian terrain, rocks are the major features shown in the rover images. It is desirable to extract, model and match rocks shown in ground images from multiple viewpoints so that they can serve as cross-site tie points. Existing rock-detection methods are aimed at detecting and modeling most of the rocks suitable for autonomous geological analysis. Gor et al. [19] developed a rock-detection method that uses image intensity information to detect small rocks and range information to detect large rocks from Mars rover images. Using this method, the shape of the extracted large rocks is modeled by metrics such as eccentricity, ellipse error, 2D sphericity, and 2D angularity [20]. CMU researchers developed a rock-detection method based on segmentation, detection, and classification using texture, color, shape, shading, and stereo data from the Zoë rover [21]. They also developed a multiple-view detection method.

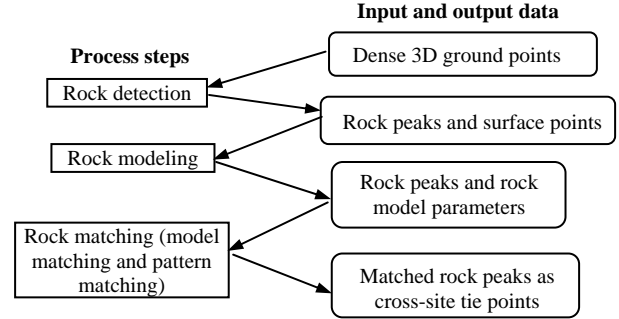


Fig. 1. Diagram of automatic cross-site tie-point selection.

Fig. 1 shows the OSU approach to cross-site tie-point selection based on rock modeling and rock matching. In this approach, rocks are detected using peak and surface point information extracted from dense numbers of ground points generated from stereo images acquired at each site. After detection, a number of analytical surface models, such as cone and spheroid, are used to fit the rock. Each rock is represented by a surface model that best fits the extracted rock surface points. After rock modeling, matching of rocks from two sites are further carried out by a comparison of individual rock models as well as of the two global rock (peak) distribution patterns from the two sites. Finally, the matched rock peaks are utilized to link rover images and to build the image network. More details on rock extraction, modeling, and matching are given in the next few subsections.

### A. Rock Extraction

1) *Extraction of Rock Peaks*: Rock peaks are extracted as local maxima from the densely distributed ground points. These three-dimensional ground points result from two steps in image matching: interest-point matching and dense image-point matching. Interest points are usually terrain features such as rock peaks, sharp corners, and ridge points. They are extracted from stereo images at each site using a Förstner interest operator. Cross-correlation is used to match these extracted interest points, which are then further refined by verification of parallax consistency and outlier elimination [14] [18]. In order to obtain enough surface points for most of the extracted rocks, a TIN (triangulated irregular network)-based dense image matching is performed for each stereo image pair to improve the terrain model. This is performed using either a 3×3 or a 5×5 grid size. After dense matching, dense 3D ground points are calculated through spatial intersection of conjugate image points.

2) *Extraction of Rock Surface Points*: Rock surface points are needed in addition to the rock peak in order to fit an analytical rock model to and describe the size of any rock. Starting from the rock peak, a 3D plane is estimated using those terrain points within an area of either 70cm×70cm or 2m×2m from the rock peak, with the

horizontal distance depending on the distance from the rock peak to the camera center. The initial rock height  $H$  is calculated as the perpendicular distance from the peak to the fitted plane. Surface points are searched for iteratively among the candidate points above the fitted plane using a dynamic search range. Fig. 2 gives examples of the extracted rock peaks and surface points for rocks with different sizes and shapes. Green dots show the rock peaks, and red dots show the extracted surface points.

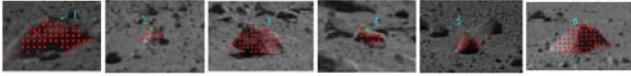


Fig. 2. Examples of extracted rock peaks (green dots) and rock surface points (red dots) for six different rocks.

The above method was successfully applied to extract the peaks and surface points for various types of rocks found about 20 m from the rover. These include large rocks of approximately 0.5m in height. The rock extraction algorithm met difficulties when dealing with a rock complex where a number of rocks stand closely together so that severe occlusions block some rock peaks and surface points. However, as long as a sufficient number of rocks can be extracted and matched between two sites, the incremental BA can be achieved.

## B. Rock Modeling

Assuming that a rock is symmetric based on the rock peak and the surface points extracted from the side visible to the camera, we can model it using a 3D analytical surface model (hemispheroid, semi-ellipsoid, cone, or tetrahedron). More information about the modeling equation, linearization, and least-squares solution can be found in [17]. To evaluate the fitting accuracy of each model for a particular rock, an RMS error is calculated from the differences of height  $z$  of the surface points, that is

$$RMS = \sqrt{\frac{(z_i - z_{i,model})^2}{n}} \quad (1)$$

where  $z_i$  is the height value of the  $i$ th surface point, and  $z_{i,model}$  is the height value calculated from the fitted model.

Table I  
Estimated model parameters and RMS errors of rocks in Fig. 2

ID	r/a (cm)	b (cm)	h (cm)	$\phi$ (radians)	RMS (cm)	Model Type
1	40.7	29.2	22.8		3.8	Ellipsoid
2	8.3		8.3	0.5	0.9	Tetrahedron
3	32		28.1	1.3	5.8	Tetrahedron
4	15.4		15.6		0.2	Hemispheroid
5	24.1		27.4		3.9	Cone
6	41.6		21.6	1.06	3	Tetrahedron

Table I gives the estimated model parameters as well as the associated RMS errors of the best-fitting models (those

with the minimum RMS error among the four models) for the six rocks in Fig. 2. In this table, the parameter  $r$  is the radius of the hemispheroid, the radius of the bottom circle of the cone, or the radius of the enclosing circle of the bottom triangle of the tetrahedron, depending on the case. The variables  $a$  and  $b$  are the semi-major and semi-minor axes of the semi-ellipsoid,  $h$  is rock height, and  $\phi$  is the orientation angle of the bottom triangle of the tetrahedron.

To verify the rock modeling results, we compared the modeled parameters with the ground truth (manual measurements from stereo images) of 79 rocks in the area between two adjacent sites at the Spirit landing site that are 26m apart. For each rock, four metrics were compared: height, radius, surface area, and volume. On the average, the relative difference between modeled and ground truth measurements was 25.1%, 43.7%, 57.1%, and 103.4% in height, radius, surface area, and volume, respectively. Additional details of this comparison are shown in [17]. It is obvious that among the four metrics, height is the most reliable and, therefore, the most comparable parameter. The very high difference in volume suggests that it should not be used for comparison. This verification result is important for designing the following rock-matching algorithm with various models.

## C. Rock Matching

Rock matching is where this approach determines which corresponding rocks can serve as tie points between two consecutive sites. Difficulties in rock matching are caused by visibility and/or occlusion, reliability of the rock modeling, and the stereo ranging capability [17].

Rock matching goes through two stages: pattern matching, which considers the global offset between the distribution of two sets of rocks from two sites, and model matching, which is the comparison of a single rock's individual similarity with potential corresponding rocks from the adjacent site.

Pattern matching compares the two geometric distributions of rock peaks from the adjacent sites. In principle, a rigid transformation including three rotations and a 3D translation can depict the relationship between two corresponding rock distribution patterns derived from the two sites. Based on extensive experiments using Spirit rover data, it was found that the rotational differences are insignificant. Consequently, a 3D translation is employed in rock-pattern matching. This makes the pattern matching process computationally more efficient.

For rock-model matching, a set of extracted candidate rocks at the adjacent site are individually compared with each significant rock extracted at the current site using the objective function

$$Z = c_1f_1 + c_2f_2 + c_3f_3 \quad (2)$$

where  $f_1$ ,  $f_2$ , and  $f_3$  are the relative differences (in percentage) of height, radius, and surface area between the two rocks calculated from the two rock models. The coefficients  $c_1$ ,  $c_2$ , and  $c_3$  are the relevant weights, which are set to 1/2, 1/3, and 1/6 based on the results of the rock model verification described above. The most comparable parameter height is given the largest weight here. The rock of the adjacent site with the minimum value of  $Z$  in Eq. 2 is considered a match.

In both rock-pattern matching and rock-model matching, there are cases of multiple matches, i.e., when a rock from one site has more than one corresponding rock candidate from the other site. To eliminate multiple matches, only the one “best” match is kept. This would be the match that generates the maximum count in rock-pattern matching, or the match with the minimum objective function value in rock-model matching. The final matching results are the combination of the outputs of the two methods. Only the rocks that pass both matching methods are considered to be matched rock pairs, i.e., the rock at one site is matched with a rock at other site both in pattern matching and model matching.

#### D. Fault Detection

In the process of cross-site tie-point selection, a fault detection algorithm is applied in order to assure that the software system mitigates failures and meets the needs for long-range rover localization. The cross-site tie-point selection software system should determine a fault if the traverse leg length is too long (>30m for Navcam), if the number of rocks extracted in the overlapping area is insufficient, if the number of extracted significant rocks is insufficient, or if there are too few rocks in the final matching result. The strategy has been applied and verified using MER Spirit data and Silver Lake field test data. In the future, additional situations will be considered and added to the strategy. Also, the theory of fault detection based on the statistic analysis is being developed and tested.

### III. RESULTS

The developed cross-site tie-point selection method has been extensively tested using MER data acquired by the Spirit rover. Furthermore, we conducted a field test at Silver Lake, CA in January 2007. Along this 5.5km traverse, VO images were taken continuously at a rate of 0.5 frames per second and BA panoramic images were taken at the ends of traverse segments (typically 20~30 meters). Differential GPS (DGPS) was employed to measure the rover positions at a data rate of 2Hz, which matches the VO image acquisition rate. The DGPS-

determined rover positions will be used as ground truth to evaluate the localization accuracy of VO and BA and their integration. We are currently testing our software using the field test data.

Fig. 3 shows an example of rock peaks automatically extracted from MER Navcam images for cross-site tie-point selection. The two sites from the Spirit rover landing site, 9600 and 9700, are 26m apart. There are 37 peaks extracted from Site 9600 (green triangles) and 34 from Site 9700 (red triangles) shown. The location of the rover location at sites 9600 and 9700 are marked as dots. Fig. 4 gives the 7 correct matching result of this test pairs. Fig. 5 also shows the 7 matched rocks on the image mosaics of sites 9600 and 9700.

Fig. 6 gives another example of the tie points automatically selected using images acquired at the Silver Lake field test. These two sites are sites Tue-am-2b-10 and Tue-am-2b-09 (16m apart)

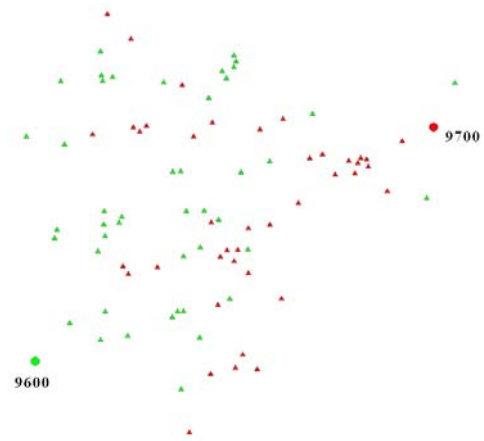


Fig. 3. Peaks extracted from two Spirit rover sites, 9600 and 9700.

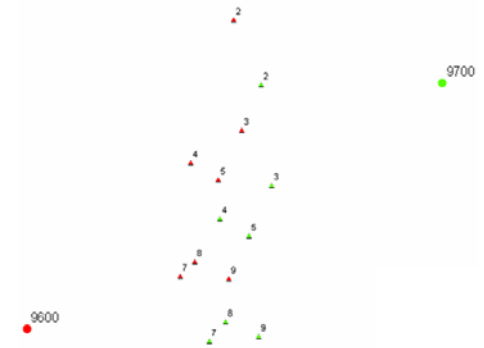


Fig. 4. Automatically matched rocks selected as cross-site tie points at MER Spirit rover sites 9600 and 9700 (labeled with the same identification numbers).

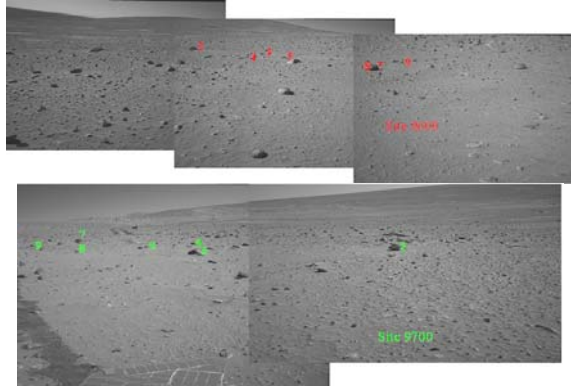


Fig. 5. Automatically matched rocks (tie points) shown on the image mosaics of sites 9600 and 9700 (labeled with the same identification numbers).

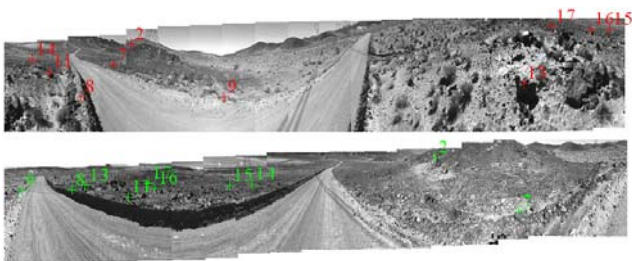


Fig. 6. Automatically matched rocks (tie points) shown on the image mosaics of two adjacent panoramas at the Silver Lake test sites (labeled with the same identification numbers).

#### IV. CONCLUSIONS AND FUTURE RESEARCH

Automatic tie-point selection is a key process for implementing the proposed autonomous Mars rover localization method. This process is realized by rock extraction, rock modeling, and rock matching using images acquired at multiple rover sites. To eliminate potential mismatches in rock matching, the complementary rock-model and rock-pattern matching methods can be employed. Also, fault detection strategies based on statistic analysis of the test data are being developed and tested. Test results using MER data show that the proposed method is effective for medium-range (up to 26m) traverse segments. Currently, we are testing our software using data acquired during a recent field test at Silver Lake, CA. The achieved cross-site tie-point selection results will be used in the onboard integration of BA and VO methods for long-range autonomous rover localization.

#### ACKNOWLEDGMENT

Part of this work is being performed at the Jet Propulsion Laboratory, California Institute of Technology, under a contract with the National Aeronautics and Space Administration. Funding of this research by the Mars Technology Program of NASA/JPL is acknowledged.

#### REFERENCES

- [1] R.E. Arvidson, et al., "Initial localization and physical properties experiments conducted by Spirit at Gusev Crater," *Science*, Special Issue on MER 2003 Mission, 305(5685), pp. 821-824, doi: 10.1126/science.1099922, 2004.
- [2] R. Li, K. Di, L.H. Matthies, R.E. Arvidson, W.M. Folkner, and B.A. Archinal, "Rover localization and landing site mapping technology for 2003 Mars Exploration Rover mission," *Photogrammetric Engineering & Remote Sensing*, 70(1), pp. 77-90, 2004.
- [3] R. Li, S.W. Squyres, et al., "Initial results of rover localization and topographic mapping for the 2003 Mars Exploration Rover mission," *Photogrammetric Engineering & Remote Sensing*, Special Issue on Mapping Mars, 71(10), 1129-1142, 2005.
- [4] D.J. Spero, "A review of outdoor robotics research," *Technical report MECSE-17-2004*, Department of Electrical and Computer Systems Engineering, Monash University, Melbourne, Australia, November 2004.
- [5] R. Volpe, T. Litwin, and L.H. Matthies, "Mobile robot localization by remote viewing of a colored cylinder," *Proc. International Conference on Robots and Systems (IROS)*, Pittsburgh, PA, August 1995.
- [6] C. Olson, and L. Matthies, "Maximum likelihood rover localization by matching range maps," *Proc. IEEE International Conference on Robotics and Automation*, Lueven, Belgium, May 1998.
- [7] C.F. Olson, L.H. Matthies, M. Shoppers, and M. Maimone, "Rover navigation using stereo ego-motion," *Robotics and Autonomous Systems*, 43(4), pp. 215-229, 2003.
- [8] D. Wettergreen, N. Cabrol, J. Teza, P. Tompkins, C. Urmsen, V. Verma, M.D. Wagner, and W.L. Whittaker, "First experiments in the robotic investigation of life in the Atacama Desert of Chile," *IEEE International Conference on Robotics and Automation*, Barcelona, Spain, April 2005.
- [9] E. Mauratte, "Mars rover autonomous navigation," *Autonomous Robots*, 14(2-3), pp. 199-208, 2003.
- [10] R. Li, F. Ma, F. Xu, L.H. Matthies, C.F. Olson, and R.E. Arvidson, "Localization of Mars rovers using descent and surface-based image data," *Journal of Geophysical Research - Planets*, 107(E11), F10D 4.1 - 4.8, 2002.
- [11] L. Matthies, E. Gat, R. Harrison, B. Wilcox, R. Volpe, and T. Litwin, "Mars microrover navigation: performance evaluation and enhancement," *Autonomous Robots*, 2(4), pp. 291-311, 1995.
- [12] M. Maimone, A. Johnson, Y. Cheng, R. Willson, and L. Matthies, "Autonomous navigation results from the Mars Exploration Rover (MER) mission," *Proc. 9th International Symposium on Experimental Robotics (ISER)*, Singapore, June 2004.
- [13] R. Li, B.A. Archinal, et al., "Rover localization and topographic mapping at the landing site of Gusev Crater," *Mars. Journal of Geophysical Research - Planets*, Special issue on Spirit rover, 111(E02S06), doi:10.1029/2005JE002483, 2005.
- [14] K. Di, F. Xu, J. Wang, X. Niu, C. Serafy, F. Zhou, R. Li, and L. Matthies, "Surface imagery based mapping and rover localization for the 2003 Mars Exploration Rover mission," *Proc. ASPRS 2005 Annual Conference*, Baltimore, MD, 2005 (CD-ROM).
- [15] K. Di, R. Li, L.H. Matthies, and C. F. Olson, "A study on optimal design of image traverse networks for Mars rover localization," *Proc. ACSM-ASPRS, 2002 Annual Conference*, Washington, D.C, 2002 (CD-ROM).
- [16] R. Li, and K. Di, "Rover traverse design and error analysis," *Technical report submitted to JPL Mars Technology Program*, Columbus, OH: Mapping and GIS Laboratory, CEEGS, The Ohio State University, February 2005.
- [17] R. Li, K. Di, A.B. Howard, L. Matthies, J. Wang, and S. Agarwal. "Rock modeling and matching for autonomous long-range Mars rover localization," *Journal of Field Robotics: Special Issue on Space Robotics*, vol. 24, Issue 3, pp. 187-203, March 2007.
- [18] F. Xu, "Mapping and localization for extraterrestrial robotic explorations," *Ph.D. Dissertation*, The Ohio State University, Columbus, OH, 2004.

- [19] V. Gor, R. Castano, R. Manduchi, R.C. Anderson, and E. Mjolsness. "Autonomous rock detection for Mars terrain," Paper presented at *AIAA Space 2001—Conference and Exposition*, Albuquerque, NM, August 2001.
- [20] R. Castano, R.C. Anderson, J. Fox, J. Dohm, A.F.C. Haldemann, and W. Fink, "Automating shape analysis of rocks on Mars," Paper presented at *the 33<sup>rd</sup> Lunar and Planetary Science Conference*, Abstract No. 2000, Lunar and Planetary Institute, Houston, TX, March 2002.
- [21] D.R. Thompson, S. Niekum, T. Smith, and D. Wettergreen, "Automatic detection and classification of geological features of interest," In *Proceedings of the IEEE Aerospace Conference*, Big Sky, MT, March 2005.